Surface & Coatings Technology 458 (2023) 129384

Contents lists available at ScienceDirect

Surface & Coatings Technology

journal homepage: www.elsevier.com/locate/surfcoat

Plasma electrolytic oxidation treatments for bimetallic substrates enabling sustainable procedures for automotive painting

Norica Godja [a], Luka Payrits [a], Markus Ostermann [a], Andreas Schindel [a], Markus Valtiner [a,b], Christian M. Pichler [a,b,*]

[a] Centre of Electrochemical and Surface Technology, Viktor Kaplan Straße 2A, 2700 Wiener Neustadt, Austria
[b] Institute of Applied Physics, TU Wien, Wiedner Hauptstraße 8-10, 1040 Wien, Austria

ARTICLE INFO

Keywords:
Plasma electrolytic oxidation
Multi-material composites
Lightweight alloys
Corrosion protection

ABSTRACT

Magnesium- or Aluminium based lightweight alloys are increasingly utilized in the automotive sector. To ensure corrosion protection of these lightweight alloys, plasma electrolytic oxidation (PEO) can be utilized to from protective layers in an efficient manner on those lightweight alloy materials. In real vehicles often a blend of joined materials is used and it must be evaluated if the joined material combinations can be subjected directly to corrosion protection treatments or if separated treatments are necessary for different materials, which would significantly enhance production costs. In this study we investigate the feasibility of the PEO process for already joined Al-alloy and Mg-alloy materials. Special focus is put on the compatibility with subsequent cathodic dip coating (CDC) processes and the corrosion resistance of the coated materials was evaluated, which is highly relevant for applications in vehicles. We provide characterization of the formed PEO layers and could demonstrate different layer formation behaviour and composition, depending on the alloy material. It could be also shown that Mg-alloy and Al-alloy materials joined by gluing and riveting can be subjected to the PEO process, resulting in effective, simultaneous protective layer formation on both materials. Finally, it is demonstrated that the joined and PEO treated materials exhibit excellent compatibility with the cathodic dip coating process and that previous PEO treatment results in better corrosion resistance also for cathodic dip coated samples.

1. Introduction

The reduction of CO_2 emissions to reach the climate targets is a major incentive for the automotive sector to implement novel technologies and materials to reach these goals [1]. The share of lightweight materials in car manufacturing has been steadily increasing over the last years, as weight reduction relates directly to reduced fuel consumption. A weight reduction of 1 kg increases the milage of a 1000 kg car by 0.016 km/L fuel [2]. Especially, aluminium- and magnesium-based alloys are intensively investigated, and novel alloy compositions are developed for implementation in car manufacturing [2,3]. Due to their various mechanical properties the alloys are utilized for different parts of the car. The growth of aluminium alloys in car manufacturing has been driven by the application as castings for the engine. But recently aluminium has been also used for Body-in-white (BIW) applications [4]. The lightweight alloys must meet several requirements for enabling their widespread utilization in car manufacturing: meet the desired mechanical properties, formability, manufacturability, joining properties, price, recyclability, and corrosion resistance. Combining the various available materials allows to harness each of their particular strengths [5]. The resulting multi-component cars bring certain challenges with them, especially regarding corrosion as galvanic corrosion can occur by combining various materials with different properties [6,7].

To prevent these corrosion phenomena, adjusted coating and painting processes are required. Especially for multi-material cars, coating processes are required that are compatible with as many materials as possible. For lightweight materials such as aluminium- or magnesium-based alloys, anodizing or plasma electrolytic oxidation (PEO) are utilized for surface treatment, to avoid material degradation by corrosion or wear [8–10]. In both methods an anodic current is applied at the metal to form passivating metal oxides on the surface. For PEO, however, the applied voltage is significantly higher (range of several 100 V). These high voltage pulses lead to micro discharges (time range of ms-µs) generating extremely high temperatures [11,12]. Thereby the metal

* Corresponding author.
E-mail address: christian.pichler@cest.at (C.M. Pichler).

https://doi.org/10.1016/j.surfcoat.2023.129384
Received 3 February 2023; Received in revised form 20 February 2023; Accepted 21 February 2023
Available online 26 February 2023

surface engages in chemical reactions with the electrolyte components and forms thick metal oxide layers. The utilization of additives in the electrolyte solution (silicates, phosphates, aluminates, or different types of particles) can improve the structure, resistance, and stability of the PEO layers [13–16]. For example, the combination of borosilicate and SiC particles as additives can improve the corrosion and wear resistance of the formed PEO layers on AZ91D Mg alloy [17].

PEO has been deemed suitable for the treatment of joined light-weight materials such as Al, Ti or Mg based alloys [18–21]. These findings are relevant for multi-material car bodies, as the PEO-treated, joined materials exhibited enhanced corrosion and wear resistance. It could be demonstrated that PEO treated AZ91D Mg alloys possess improved tribocorrosion properties [22]. So far mainly welded metal combinations were tested for the PEO treatment. Other joining processes such as riveting, or gluing have not been investigated for their compatibility with PEO treatment, although they are also relevant for automotive industry [23,24]. For applications in car manufacturing subsequent process steps, such as painting, are highly relevant, however they are rarely considered when studying PEO of lightweight metal alloys.

This study therefore investigates the behaviour of light weight alloy combinations joined by gluing and riveting in the PEO process. By introducing the stainless-steel rivet, a complex three-material interface is formed, which has not been investigated in detail previously. As light weight alloys, the aluminium alloy AA6082 and the magnesium-based alloy AZ91 are utilized and the PEO treatment is conducted for the already joined three-material compound (AA6082 + AZ91 + stainless-steel). The microscopic structure and corrosion resistance properties of the formed PEO layers are investigated. For applications in car manufacturing, it is crucial that the PEO treated materials are compatible with standard cataphoretic painting. Therefore, the PEO treated material compounds are cataphoretically painted and the corrosion and structural properties of the painted components are evaluated as well. The compatibility of the PEO treated materials with cataphoretic painting decides, if those materials can be used for actual manufacturing processes [25–27].

2. Experimental

2.1. Materials

Aluminium alloy AA6082 (0.4–1 % Mn, 0–0.5 % Fe, 0.6–1.2 % Mg, 0.7–1.3 % Si, Cu < 0.1 %, Zn < 0.2 %, Ti < 0.1 %, Cr < 0.25 %, Al balance) and Magnesium alloy AZ91 (8.3–9.7 % Al, 0.3–1.0 % Zn, 0.2 % Mn, 0.01 % Si, 0.03 % Cu, 0.002 % Ni, 0.005 % Fe, Mg balance) were obtained from LKR Ranshofen and Neuman Aluminium respectively. Ethanol, Acetone, Acetic acid, $NaNO_3$, $KMnO_4$, $LiNO_3$, Na_3VO_4 were obtained from Sigma Aldrich or Alfa Aesar and used as received.

2.2. Sample pretreatment and formation of PEO layers

The light weight alloy plates (5 × 5 cm) were joined using single strap lap riveting plus gluing. The joined plates were precleaned by ultrasonication in EtOH/Acetone solution for 2 min. Afterwards the samples were washed with Acetone and dried immediately. Finally, the samples were immersed in 3 % Bonderite C-AK 5948R Aero (alkaline cleaning – from Henkel) stirred with 250 rpm, at 65 °C for 15 min. Before the PEO process, three different pre-treatment protocols were applied:

For the first method ("V1") the samples were immersed into a pickling solution of Acetic acid (190 g L^{-1})/$NaNO_3$(30 g L^{-1}) at room temperature (20 °C) for 10 s at a stirring speed of 250 rpm. After that the samples were washed with distilled H_2O and subjected to plasma electrolytic oxidation. In the second method ("V2") a conversion layer was formed on the metal surface using an electrolyte (Sealing B) consisting of 19 g L^{-1} $KMnO_4$, 3.5 g L^{-1} $LiNO_3$, and 6 g L^{-1} Na_3VO_4 at 50 °C for 10 min with a stirring speed of 250 rpm [28]. The samples were washed with distilled H_2O after the coating treatment and directly used for cathodic dip coating.

For the third method ("V3") the sample underwent again conversion layer formation as described for sample "V2" but was followed then by plasma electrolytic oxidation and cathodic dip coating.

For the plasma electrolytic oxidation 7 l of electrolyte was prepared containing 6 l of distilled H_2O, 210 g NaOH, 1281 g $Na_2B_4O_7$*$10H_2O$ and 1278 g Na_4SiO_4. The process was operated at a constant potential of 148.6 V and a maximal current density of 0.6 A cm^{-2}. The process lasted for 10 min at a stirring speed 400 rpm. The temperature during PEO was held between 5 and 7 °C.

For cathodic dip coating a commercial WK-LACKBAD (FreiLacke - Emil Frei GmbH & Co. KG) was used. Process time was 10 min on 33 °C at 300 rpm. The air bubbles were removed from the surface using distilled water. Afterwards the samples were dried at 160 °C.

2.3. Sample characterization

Corrosion resistance was evaluated with impedance measurements performed with a Biologic SP-240 Potentiostat. A three-electrode setup was used with the joined metal plates as working electrodes, a Pt-counter electrode (5 cm^2) and an Ag/AgCl (3 M KCl) reference electrode in 3.5 wt% aqueous NaCl solution in the frequency range of 10^5–10^{-2} Hz with an amplitude of ±10 mV at the open circuit potential (OCP). The OCP was recorded for 1 h prior to impedance measurements. Measurements were performed three times to ensure reproducibility.

A Fischer Dualscope FMP40 FKC30 dry film thickness gauge was applied to determine the thickness of the paint layer of the cathodic dip coating. For the magnesium (AZ91) and aluminium (AA6082) plates the ETA 3.3 sensor was used. For calibration, non-threated plates were used with two different calibration foils of 24.1 μm and 120 μm (for magnesium), 10.8 μm and 24.1 μm (aluminium), five points for each calibration per foil, respectively.

A scanning electron microscope FE-SEM "ΣIGMA HD VP" from ZEISS equipped with a TEAM Pegasus EDX system and TEAM Octane Plus SSD detector (from EDX) was deployed for qualitative surface analysis. Secondary electron (SE) and back scattered electron (BSE) images were obtained with 15 kV and a working distance of 8.4 mm. In order to examine the element distribution on the surface, EDX mappings were performed on a 1 mm × 1 mm area of each specimen (20 kV, 256 × 200 matrix, dwell time: 200 μs/point).

The cross sections of the PEO treated samples were cut, embedded in epoxy resin and polished before SEM analysis.

The salt spray test was performed in a Weisstechnik SaltEvent chamber, where the inner temperature was 35 °C during the process and the temperature of the humidifier was 49 °C. The concentration of the NaCl solution was 4.4 %. Tests were performed with three samples to ensure reproducibility.

3. Results and discussion

In this study three different pre-treatments for joined Al and Mg compounds are investigated. Especially, the influence of PEO treatment for the material couples on the final compound stability is of main relevance. Samples V1 and V3 both underwent a PEO process, while sample V2 is only protected by a chemical conversion layer, to serve as benchmark for the PEO processed samples. In Fig. 1 the current response over time is shown for the PEO treated samples. Samples V1 and V3 differ in their pre-treatment, as V1 underwent a short time pickling treatment and V3 was subjected to conversion layer formation (same as V2), before being subjected to the PEO treatment. Furthermore, it must be emphasized that in this case the pre-treated and already joined (riveted and glued) Mg-alloy + Al-alloy samples were subjected to a constant potential PEO treatment, for a simultaneous formation of the protective layer on both alloys.

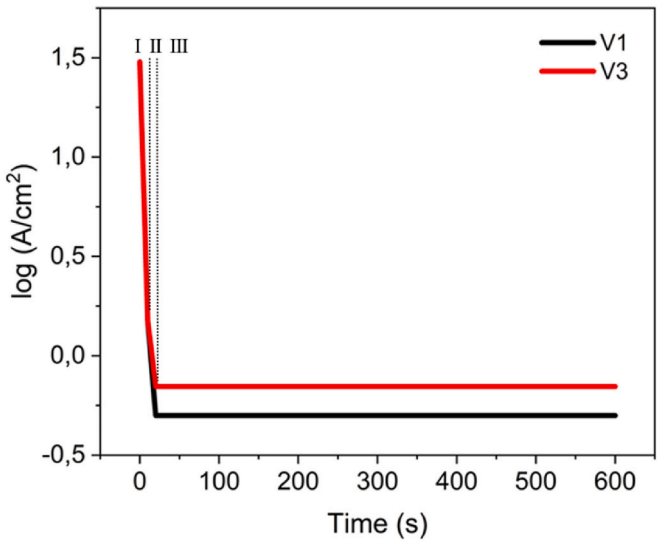

Fig. 1. Current density during the PEO process for joined Mg + Al alloys, V1: pickling pre-treatment, V3: Conversion layer formation pre-treatment. Different stages of PEO layer formation (I, II, III are marked for the red curve). (For interpretation of the references to colour in this figure legend, the reader is referred to the web version of this article.)

Both samples show a rapid decline of the current from 0.43 A cm^{-2} and 0.85 A cm^{-2} as starting values to 0.007 A cm^{-2} and 0.01 A cm^{-2} for V1 and V3 in the first 20 s of the PEO process. The rapid current drop can be explained by the immediate formation of the protective layer. The progression of the curve allows the identification of the different stages of PEO layer formation. Stage *I* resembles conventional anodization, characterized by the growth of a thin oxide layer. Corresponding with the growth of this oxide layer the measured current decreases (in the more common constant current PEO process, the voltage would show a linear increase during that stage until reaching the breakdown voltage, indicating to the dielectric breakdown of the oxide film.) In stage *II* small sized white discharges begin to appear on the substrate surface, indicating spark anodization. This is followed by stage *III*, where micro arc oxidation commences. Generally, the different stages of the PEO are better visible in constant current experiments. The constant potential conditions used in this study, result in a greater number of small sparks and discharges, which allows a gentler oxide growth. However, the discharge appearance differs from the constant current conditions, especially in the later stages [29,30].

Compared with other examples from literature, the applied constant voltage of 148.6 V is comparably low, resulting in smaller current densities. Studies with Mg-alloys at 490–500 V gave current densities of approx. 200 mA cm^{-2} [19]. The lower voltage has advantage of reduced energy consumption and more gentle reaction conditions for the slower formation of the protective layer. The constant voltage mode was applied to avoid discharge damages or oxidation of non-oxides inclusions. It has been reported that the constant voltage mode is generally resulting in lower thicknesses of the PEO formed layer [10]. However, in this case the PEO-layer shall mainly facilitate a stable connection with the cathodic dip coating (CDC) layer, and not act as protection layer itself. Hence, the potentially lower layer thickness is of no major concern.

3.1. Characterization of layers

The protective layers were investigated with scanning electron microscopy (SEM). When comparing the samples, it must be considered that V1 and V3 underwent PEO treatment, while V2 was subjected only to conversion layer formation. The riveted samples are shown in Fig. 2, and clearly show different optical appearance for the treated samples. The different pre-treatments for V1 and V3 had no major influence on the final PEO barrier layer microstructure, as was determined with SEM. However, the morphology on the Mg-alloy and the Al-alloy can be easily differentiated. The Al surface (left in Fig. 3) shows a layer with medium roughness and few pores in the size range of 1–5 μm for V1 and V3. The Mg-alloy surface shows a complex amorphous structure with a higher number of pores and pore sizes of up to 10 μm. The distinct difference between the Al and Mg alloy is caused by the different behaviour and chemical reactivity of the two alloys during the PEO process. For the sample V2, no PEO treatment was performed and only a conversion layer has been formed, which has a significantly different surface morphology, compared with the PEO treated samples. For the Al-alloy, the surface is smoother and less porous compared with the PEO treated samples. The Mg alloy shows no thick barrier layer, but the blank metal surface with the distinct structure from cutting and polishing the sample is clearly visible.

The chemical composition of the material surface can be determined with energy dispersive X-ray spectroscopy (EDX). In Table 1 elemental composition for the different samples and the respective alloys is given. For the Al-alloys the chemical composition of all samples is very similar, regardless of an undergone PEO treatment. For the PEO treated samples V1 and V3, the Si content is slightly higher compared to V2 (3.6 % and 1.4 % vs. 0.7 %), which is not surprising as Si was present in the PEO electrolyte solution. The oxygen content was determined to be 28.7 % and 29.8 % for V1 and V3 and 24.6 % for V2 and the aluminium content was 53.8 % and 56.1 % for V1 and V3 and 57.3 % for V2. The results indicate that aluminium oxide species are present in all samples. For the PEO treated samples V1 and V3 the oxygen content is slightly higher, which might be a result of the treatment. In general, the difference in chemical composition for the Al-alloys is small for the PEO treated and untreated samples.

This changes significantly, for the Mg-alloys. The PEO treated samples V1and V3 exhibit high concentrations of Si, Na and O, 14.6 %, 11.8 %, 59.6 % and 14.1 %, 6.8 %, 60.7 % respectively. The Mg concentration

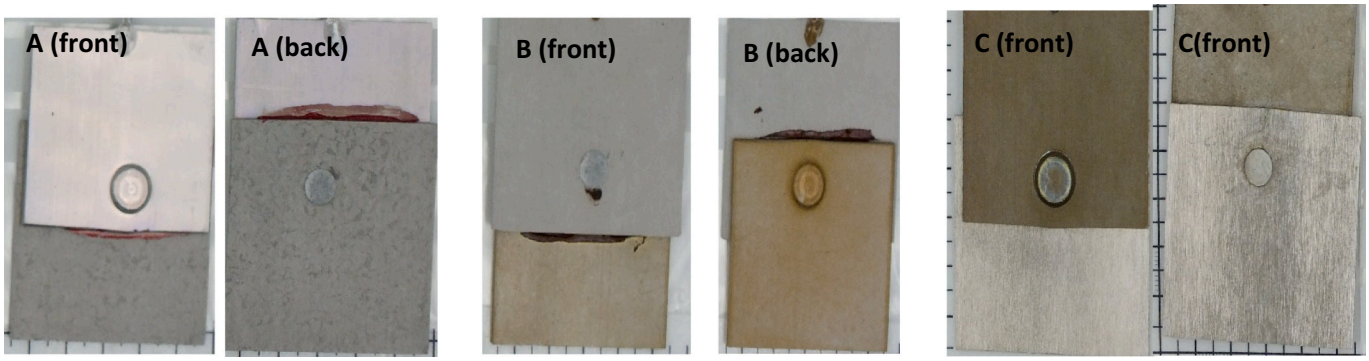

Fig. 2. Photographs of treated and glued, riveted samples, A) V1 (pickling + PEO), B) V2 (Sealing B), C) V3 (Sealing B + PEO).

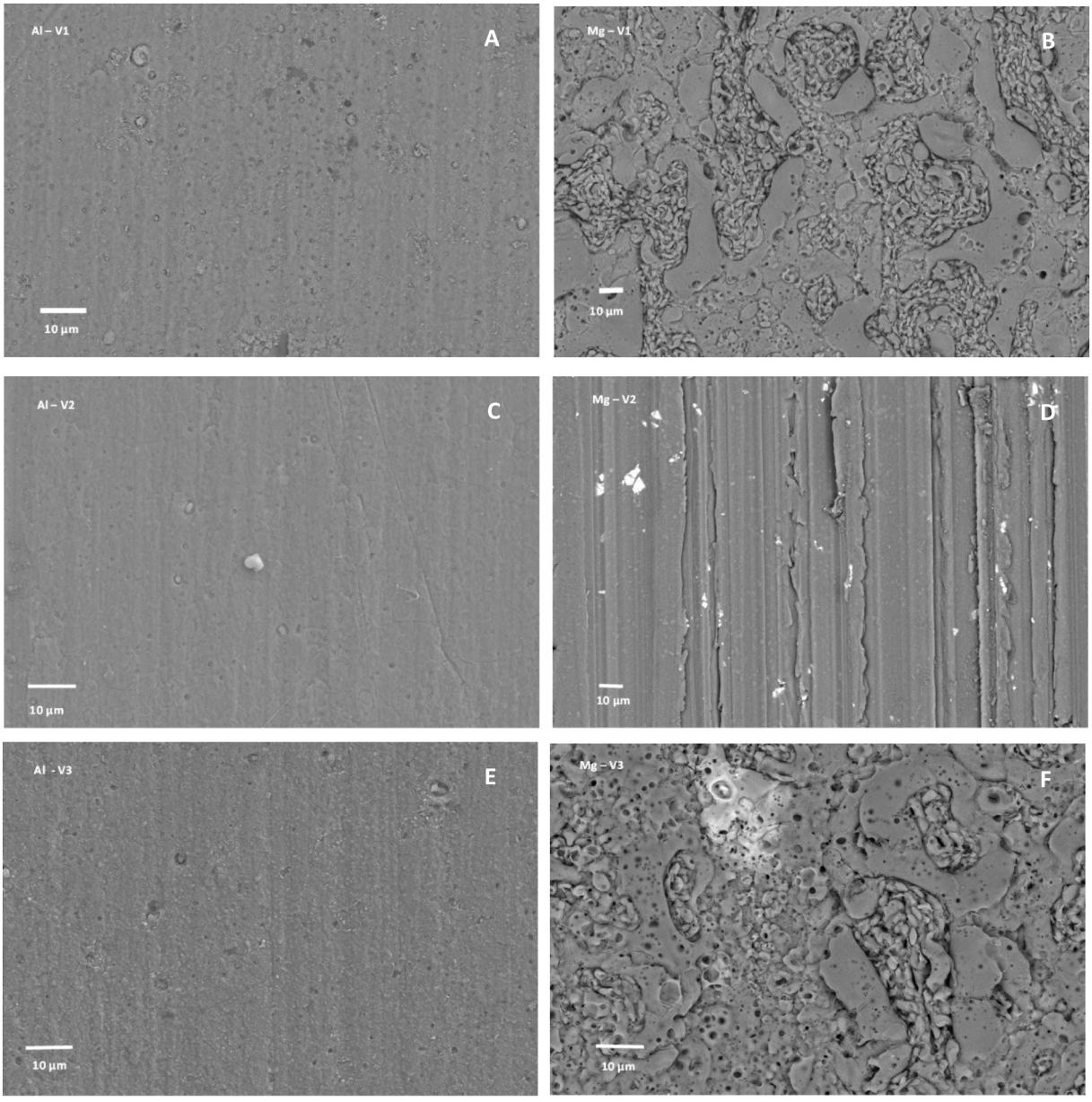

Fig. 3. SEM images of samples V1 (pictures A and B), V2 (pictures C and D) and V3 (pictures E and F), Top-down view Al-alloy (left) and Mg-alloy (right).

Table 1
Elemental composition of the samples determined by EDX in atomic %.

Sample	Al (at. %)	Mg (at. %)	O (at. %)	C (at. %)	Si (at. %)	Na (at. %)
V1 – Al alloy	53.8	1.1	28.7	11.8	3.6	–
V1 – Mg alloy	0.3	13.4	59.6	–	14.6	11.8
V2 – Al alloy	57.3	2	24.6	12.7	0.7	–
V2 – Mg alloy	5.8	70.4	7.6	15.1	0.5	–
V3 – Al alloy	56.1	1.4	29.8	10	1.4	0.7
V3 – Mg alloy	0.7	17.5	60.7	–	14.1	6.8

is with 13.4 % and 17.5 % comparably low. This indicates that a silicate rich phase was formed by the PEO process, which is also most likely responsible for the distinctive appearance of the surface. For the untreated sample V2 the Si and O concentration are significantly lower with 0.5 % and 7.6 % and no Na was detected. In contrast, the detected Mg concentration was higher, with 70.4 %. This suggests that only a thin conversion layer is present, and no other protection layer (except minor amount of surface oxides) is present.

To determine the thickness of the different layers, cross sections of the samples were prepared for SEM analysis. For the sample V1 (Fig. 4, Images A and B) a dense oxidic layer, with a thickness of approximately 200 nm was formed on the Al-alloy, by the PEO process. The PEO formed layer on the Mg-layer is with 3–5 µm significantly thicker and shows a typical appearance for PEO treated materials. It consists of an inner, dense layer with a thickness of approx. 500 nm, often termed as barrier layer. On top of that an area with a great number of larger pores, the so-called pore band, is found, which is adjacent to the outer layer, that possesses limited porosity. Pores are a common feature in PEO processed materials. Their size and extend depends on the melt flow back and

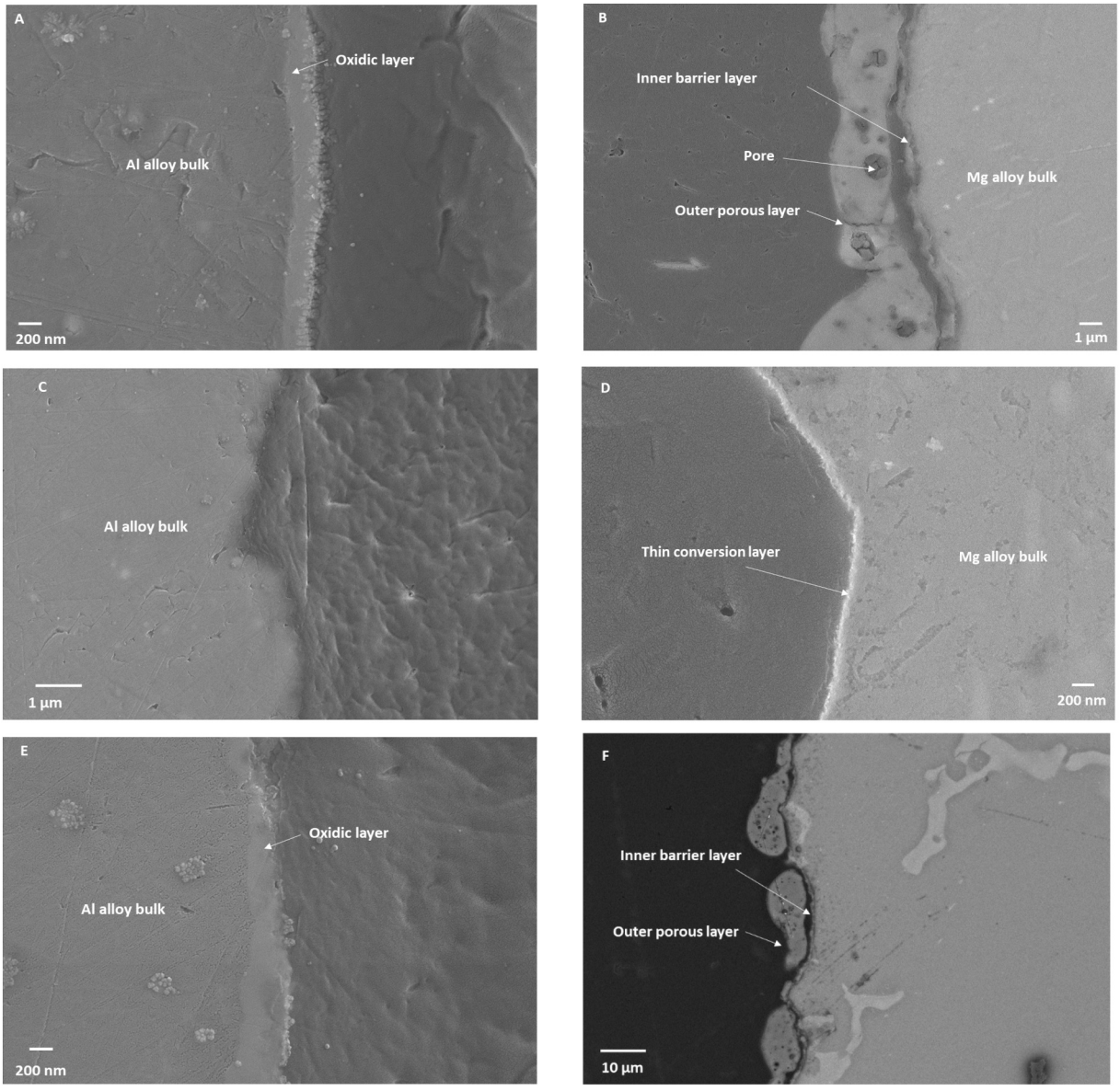

Fig. 4. SEM images of sample cross-sections V1 (pictures A and B), V2 (pictures C and D) and V3 (pictures E and F), Al-alloy (left) and Mg-alloy (right).

liquid phase sintering during repetitive discharges of the PEO process [31]. Nevertheless, pores are a potential weakness in the PEO formed layer and can potentially serve as site for corrosion attack, even though the inner layer in this case is homogeneous and dense, protecting the underlaying metal. For sample V2, no barrier layer can be found, as this sample did not undergo PEO treatment (Fig. 4, C and D). On the Al alloy, no surface layer is visible, the expected oxidic Al species on the surface are too thin and cannot be detected with the utilized magnification. For the Mg-alloy a thin, light layer can be found, most likely the oxidic conversion layer. On sample V3, thick layers, resulting from the PEO process can be found (Fig. 4, E and F). The layer on the Al alloy is with 200–400 nm slightly thicker than on sample V1 and is has a regular and dense appearance. On the Mg alloy, a significantly thicker layer array was formed, with a complete thickness of approx. 10 µm. The innermost barrier layer exhibits a dense appearance and a thickness of approx. 500 nm. On top of that the pore band is found, followed by the outer porous layer. This three-layer assembly is common for PEO treated Mg alloys, and the corrosion resistance is mainly determined by the inner barrier layer, while the outer layers are important for interactions with additional coatings [32].

The first evaluation of the produced systems before cathodic dip coating was performed with electrochemical impedance spectroscopy (EIS) (see Fig. 5 A & B). The recorded spectra were fitted via equivalent circuits (see Fig. 6) similar to circuits reported in literature [22]. Sample "V2" with the conversion layer exhibits unsignificant corrosion protection with the fitted resistances (see Table 2) being in the range of the untreated pure metal. Initial corrosion protection is achieved via PEO treatment showing increased resistance via an inner (R_3) and outer (R_2) barrier layer. Further combination of PEO and the conversion layer (V3) improves the resistance of the inner (R_4) and outer (R_3) barrier layer and indicates a significant improvement of the corrosion resistance. The increased OCP of the sample additionally underlines the corrosion resistance improvement.

The next step was the cathodic dip coating (CDC) of the joined and pre-treated samples. The polymeric CD-coating is an excellent corrosion protection, as demonstrated by the impedance spectra (Fig. 5 C & D) of the coated samples. The CD-coated samples are fitted with the same equivalent circuit model adding an EC-circuit for the CD-coating (see Fig. 6 C). The resistance values (see Table 3) are for all CD-coated samples significantly higher than the non-coated samples, which is not

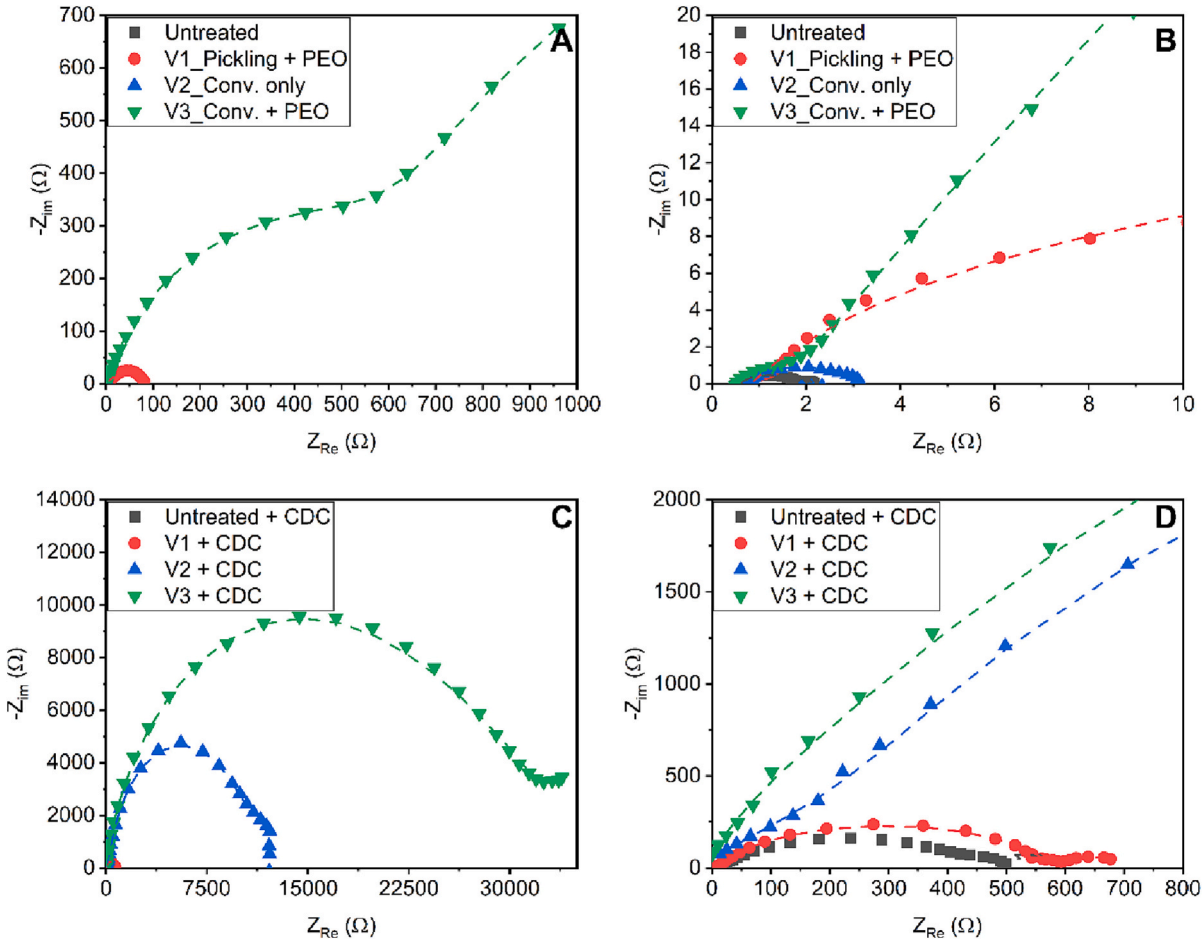

Fig. 5. Nyquist plots for the joined AA6082 + AZ91 samples in 3.5 wt% aqueous NaCl solution, A) and B) Before cathodic dip coating; C) and D) After cathodic dip coating (dashed line relates to fitted model).

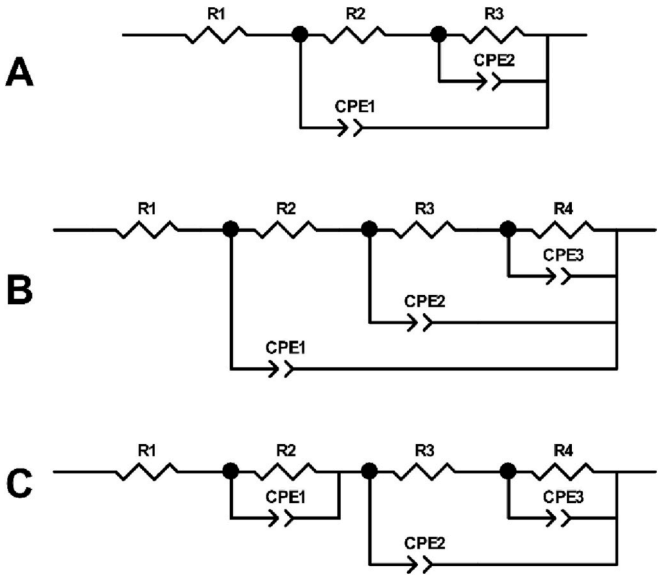

Fig. 6. Equivalent circuit (EC) models used for fitting the electrochemical impedance spectra.

surprising, as the CDC process forms a polymer layer on the metal, that acts as corrosion protection barrier.

The untreated and PEO-treated samples show low corrosion resistance with resistance in the range of 500 Ω. By addition of the conversion layer (V2 + CDC), the corrosion resistance increases significantly. This indicates improved adhesion of the CDC-layer to the substrate improving performance. Combination of the PEO- and the conversion layer ultimately improves the corrosion resistance to resistances of about 35 kΩ (R_4), showing the positive effect of the PEO pretreatment even after the coating process. The increased OCP is an additional indicator for improved corrosion protection.

The CDC layer thickness was determined with a dry film thickness

Table 2
EIS results of samples before cathodic dip coating: OCP at steady-state, used EC-model as described in Fig. 6, results of the EC fitting.

	Untreated	V1_Pickling + PEO	V2_Conv. Only	V3_Conv. + PEO
OCP vs. SHE [V]	−1.30	−1.32	−1.33	−0.89
EC-Model	A	A	A	B
R_1 [Ω]	0.62	0.83	0.63	0.57
R_2 [Ω]	1.22	27.85	0.20	1.69
R_3 [Ω]	0.39	51.18	2.33	837
R_4 [Ω]	–	–	–	1831
Q_1 [F Hz^{1-n}]	$2.56•10^{-3}$	$2.79•10^{-4}$	$2.06•10^{-3}$	$7.22•10^{-6}$
n_1	0.83	0.75	0.70	1.00
Q_2 [F Hz^{1-n}]	$4.20•10^{0}$	$4.38•10^{-4}$	$1.55•10^{-3}$	$2.32•10^{-4}$
n_2	0.71	0.91	0.87	0.79
Q_3 [F Hz^{1-n}]	–	–	–	$1.75•10^{-3}$
n_3	–	–	–	0.92
χ^2	$2.53•10^{-5}$	$3.25•10^{-3}$	$2.09•10^{-4}$	$1.36•10^{-3}$

Table 3
EIS results of samples after cathodic dip coating: OCP at steady-state, used EC-model as described in Fig. 6, results of the EC fitting.

	Untreated + CDC	V1 + CDC	V2 + CDC	V3 + CDC
OCP vs. SHE [V]	−1.32	−1.31	−1.32	−0.75
EC-Model	C	C	C	C
R_1 [Ω]	2.68	3.70	2.80	1.84
R_2 [Ω]	71.4	157	314	75.0
R_3 [Ω]	48.8	49.3	2060	192
R_4 [Ω]	382	518	10,526	36,945
Q_1 [F Hz^{1-n}]	$1.87•10^{-4}$	$2.29•10^{-3}$	$1.28•10^{-6}$	$4.65•10^{-7}$
n_1	1.00	0.78	0.71	1.00
Q_2 [F Hz^{1-n}]	$2.41•10^{-6}$	$8.90•10^{-7}$	$7.62•10^{-6}$	$2.64•10^{-6}$
n_2	0.80	0.89	0.97	0.40
Q_3 [F Hz^{1-n}]	$2.97•10^{-6}$	$1.29•10^{-6}$	$1.43•10^{-7}$	$1.26•10^{-7}$
n_3	0.84	0.87	0.92	0.91
χ^2	$1.85•10^{-4}$	$1.89•10^{-4}$	$1.51•10^{-4}$	$1.97•10^{-4}$

Table 4
Thicknesses of the cathodic dip coating layer.

Layer thickness in µm					
V1		V2		V3	
AA6082	*AZ91*	*AA6082*	*AZ91*	*AA6082*	*AZ91*
26.26 ± 0.97	28.05 ± 3.38	29.96 ± 1.82	27.66 ± 1.39	27.16 ± 1.63	26.12 ± 1.63

gauge. There were no major differences in between the different samples and alloys, as listed in Table 4. The pre-treatment conditions seem to have no significant effect on the final cathodic dip coating layer.

The results indicate that the PEO + CDC treatment can be efficiently applied for the already joined AA6082 + AZ91 samples. Considering the stainless-steel rivet to enable the joining, a complex three material interface is formed in this case. Interfaces of this type are normally prone to contact corrosion and a challenging to protect. This underlines the great potential of the PEO process, as it enabled efficient formation of protective layers for both alloys, even if they are already joined, while ensuring excellent compatibility with the CDC process.

To investigate the corrosion resistance of the dip coated samples, they were subjected to salt spray tests for a duration of 336 h (35 °C Temperature, 4.4 % NaCl concentration). Visual inspection after the salt spray tests shows small, but visible corrosion on the edges of the Mg alloy for the V1 sample, while V3 shows only minor damage on the Mg alloy. For the V2 sample the corrosion attack is stronger and further accompanied by heavy blister formation of the CD-coating of the Mg alloy. Blister and bubble formation is typically a result of increased pressure at certain points in a coating film. The increased pressure is caused by development of gas and vapor within the coating film or the substrate, caused by moisture penetration into the coating [26,33]. For Mg and Al alloys, galvanic corrosion is frequently observed, in case the corrosive medium can penetrate the coating layer and reach the metal substrate. In this case the galvanic corrosion also involves the formation of H_2 gas, which further contributes to the formation of blisters. The observation of blistering in this case, indicates that the connection between the metal surface and the CD-coating is not sufficiently strong, and water can penetrate in between those two layers and cause these destructive effects. When comparing the samples after the salt spray test, sample V3 shows the least amount of corrosion induced damage except for minor blistering on the Mg alloy, followed by sample V1 that shows corrosion on the Mg alloy, while V2 shows heavy blistering and corrosion on the Mg alloy. It is remarkable that for all samples the Al alloy shows negligible signs of corrosion. This indicates that regardless of the pre-treatment, the CD-coating possesses high affinity to the Al alloy. For the Mg severe differences between the particular pre-treatments are found. The effectiveness of the PEO treatment is demonstrated, as the PEO treated samples V1 and V3 show significantly better corrosion resistance than the non-PEO treated sample V2. It can be assumed that the surface of the Mg alloy, shows suitable affinity to the polymer coating and forms a stable interphase. Furthermore, the amorphous, slightly porous morphology of the PEO layer, might also contribute to the beneficial interactions with the coating, as the pores can serve as interlocking sites for the polymer layer. This mechanical interlocking can enhance the stability of the CDC layer. Thereby, the corrosive aqueous medium cannot penetrate the coating and reach the metal surface. Comparing, V1 and V3 with each other, it seems that the conversion layer + PEO treatment is more effective than the pickling + PEO treatment and results in more stable coating layers.

Finally, a three-material sample was prepared where AA6082, AZ91 and a zinc-coated steel were glue-riveted together, pre-treated according to the parameters of sample V3 and then cathodically dip coated. The dip coated 3-component sample was then subjected to a VDA 233–102 corrosion test, which is frequently used in automotive industry. Compared to the pure salt-spray tests in Fig. 7, the VDA test includes also non-salt spray phases and climate/temperature changes and is therefore, more relevant to assess real-world conditions. As shown in Fig. 8, no visible damage can be seen on the three-material sample after the VDA test. This is a strong indication that the described PEO treatment is suitable to treat complex multi-material compounds, relevant for car manufacturing.

4. Conclusion

We could successfully demonstrate the PEO treatment of glued and riveted Al and Mg alloys and the following conclusions could be drawn:

- The pre-joined materials can undergo PEO treatment and amorphous layers, rich in silicon and oxygen are formed on the Al and the Mg based alloy [29,34]. Pre-treatments such as pickling, or the formation of conversion layers does not influence the chemical or morphological structure of the resulting PEO layers significantly, while influence on the corrosion resistance have been found.
- The PEO layers also show some resistance to corrosion itself and after cataphoretic painting the corrosion resistance is significantly enhanced. This proves, that PEO layers are compatible with CDC and provide enhanced corrosion protection. Salt-spray corrosion tests showed that PEO treatment before cataphoretic painting, leads to better corrosion resistance of the painted samples.
- It is expected that mechanical interlocking between the CD-coating and the PEO layer contributes to the observed corrosion stability.
- A three-material combination with AA6082, AZ91 and zinc-coated steel could be demonstrated and resulted in good stability in the VDA corrosion test.
- PEO can be applied for material combinations, utilized in vehicles, and improves the corrosion stability when combined with cataphoretic painting. Since modern car bodies usually consist of a mix of materials, further tests are necessary to determine, whether these barrier coatings should be applied to the individual materials, or – in a more cost-efficient way – to joined multi-material components, as demonstrated in this study.

CRediT authorship contribution statement

Norica Godja: Conceptualization, Validation; **Luka Payrits:** Investigation, Writing; **Markus Ostermann:** Investigation, Formal analysis, Writing Visualization; **Andreas Schindel:** Investigation; **Markus Valtiner:** Conceptualization, Supervision; **Christian M. Pichler:** Conceptualization, Supervision, Writing, Validation. All authors commented and agreed on the manuscript.

Declaration of competing interest

The authors declare that they have no known competing financial

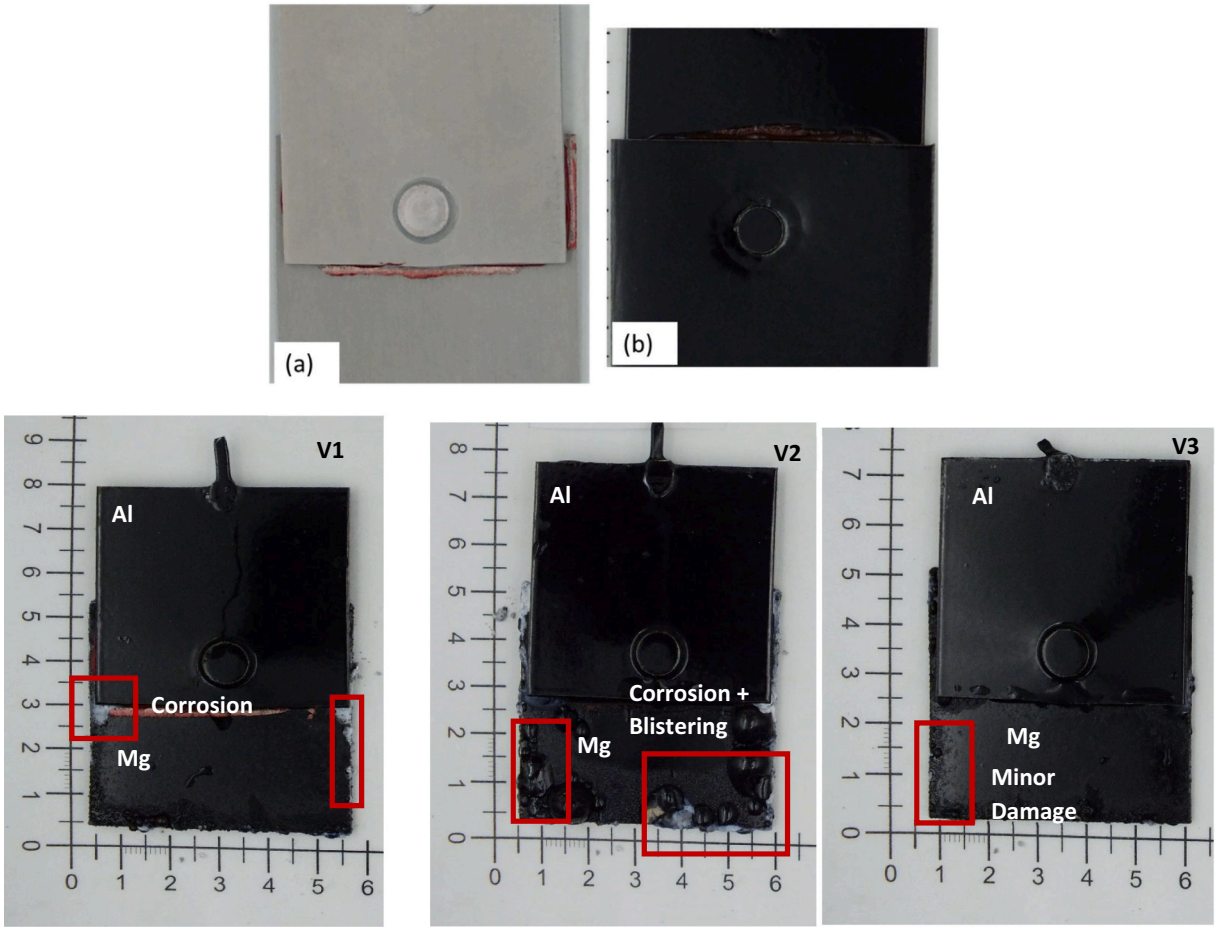

Fig. 7. Top: Sample V1 before (a) and after (b) cathodic dip coating; Bottom: Cathodic dip coated samples after 336 h salt spray tests at 35 °C with 4.4 % NaCl solution. Sample V1 (left), V2 (middle) and V3 (right), corrosion marked with red square. (For interpretation of the references to colour in this figure legend, the reader is referred to the web version of this article.)

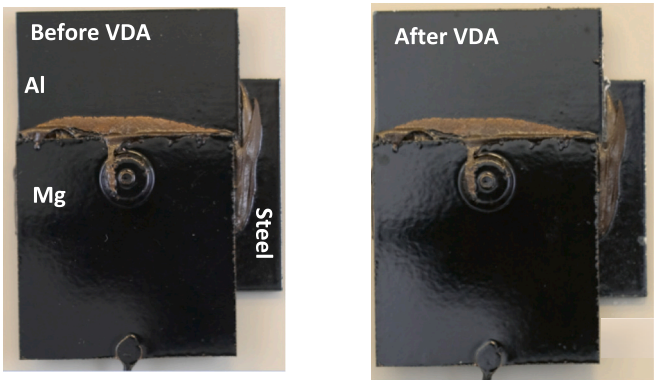

Fig. 8. Three-material component before and after VDA corrosion tests.

interests or personal relationships that could have appeared to influence the work reported in this paper.

Data availability

Data will be made available on request.

Acknowledgements

Peter Auer, Jennifer Stippich, Rudolf Vallant and Josef Domitner from the Research Group of Lightweight and Forming Technologies of the Graz University of Technology are gratefully acknowledged for joining the samples. We thank Rene Wultsch for skilful support with the SEM imaging and Jürgen Schodl for assistance with the electrochemical impedance measurements. Financial support from the Austrian Research Promotion Agency (FFG; Project Number 884352) and the COMET funding scheme is gratefully acknowledged.

References

[1] A.H. Musfirah, A.G. Jaharah, Magnesium and aluminum alloys in automotive industry, J. Appl. Sci. Res. 8 (2012) 4865–4875. http://www.worldaluminium.org.
[2] D. Kumar, R.K. Phanden, L. Thakur, A review on environment friendly and lightweight magnesium-based metal matrix composites and alloys, Mater. Today Proc. 38 (2020) 359–364, https://doi.org/10.1016/j.matpr.2020.07.424.
[3] O. Kayode, E.T. Akinlabi, An overview on joining of aluminium and magnesium alloys using friction stir welding (FSW) for automotive lightweight applications, Mater Res Express. 6 (2019), https://doi.org/10.1088/2053-1591/ab3262.
[4] M. Tisza, I. Czinege, Comparative study of the application of steels and aluminium in lightweight production of automotive parts, Int. J. Lightweight Mater. Manuf. 1 (2018) 229–238, https://doi.org/10.1016/j.ijlmm.2018.09.001.
[5] M. Patel, B. Pardhi, S. Chopara, M. Pal, Lightweight composite materials for automotive-a review, Int. Res. J. Eng. Technol. (2008) 41. www.irjet.net.
[6] A. Buling, J. Zerrer, Increasing the application fields of magnesium by ultraceramic®: corrosion and wear protection by plasma electrolytical oxidation (PEO) of mg alloys, Surf. Coat. Technol. 369 (2019) 142–155, https://doi.org/10.1016/j.surfcoat.2019.04.025.
[7] A. Mehner, A. von Hehl, H.W. Zoch, Galvanic corrosion of aluminum wrought alloys in integral hybrid components with carbon fiber reinforced plastics (CFRP) and titanium, Mater. Corros. 69 (2018) 648–660, https://doi.org/10.1002/maco.201709658.
[8] T. Arunnellaiappan, M. Ashfaq, L. Rama Krishna, N. Rameshbabu, Fabrication of corrosion-resistant Al2O3-CeO2 composite coating on AA7075 via plasma

electrolytic oxidation coupled with electrophoretic deposition, Ceram. Int. 42 (2016) 5897–5905, https://doi.org/10.1016/j.ceramint.2015.12.136.
[9] A.L. Yerokhin, X. Nie, A. Leyland, A. Matthews, Characterisation of oxide films produced by plasma electrolytic oxidation of a Ti6Al4V alloy, Surf. Coat. Technol. 130 (2000), 195206, https://doi.org/10.1016/S0257-8972(00)00719-2.
[10] D.S. Tsai, C.C. Chou, Influences of growth species and inclusions on the current–voltage behavior of plasma electrolytic oxidation: a review, Coatings 11 (2021) 1–21, https://doi.org/10.3390/coatings11030270.
[11] C.S. Dunleavy, I.O. Golosnoy, J.A. Curran, T.W. Clyne, Characterisation of discharge events during plasma electrolytic oxidation, Surf. Coat. Technol. 203 (2009) 3410–3419, https://doi.org/10.1016/j.surfcoat.2009.05.004.
[12] A.L. Yerokhin, X. Nie, A. Leyland, A. Matthews, S.J. Dowey, Plasma electrolysis for surface engineering, Surf. Coat. Technol. 122 (1999) 73–93, https://doi.org/10.1016/S0257-8972(99)00441-7.
[13] V. Birss, S. Xia, R. Yue, R.G. Rateick, Characterization of oxide films formed on mg-based WE43 alloy using AC/DC anodization in silicate solutions, J. Electrochem. Soc. 151 (2004) B1, https://doi.org/10.1149/1.1629095.
[14] F.A. Bonilla, A. Berkani, Y. Liu, P. Skeldon, G.E. Thompson, H. Habazaki, K. Shimizu, C. John, K. Stevens, Formation of anodic films on magnesium alloys in an alkaline phosphate electrolyte, J. Electrochem. Soc. 149 (2002) B4, https://doi.org/10.1149/1.1424896.
[15] X. Lu, M. Mohedano, C. Blawert, E. Matykina, R. Arrabal, K.U. Kainer, M. L. Zheludkevich, Plasma electrolytic oxidation coatings with particle additions – a review, Surf. Coat. Technol. 307 (2016) 1165–1182, https://doi.org/10.1016/j.surfcoat.2016.08.055.
[16] L. Pezzato, M. Rigon, A. Martucci, K. Brunelli, M. Dabalà, Plasma electrolytic oxidation (PEO) as pre-treatment for sol-gel coating on aluminum and magnesium alloys, Surf. Coat. Technol. 366 (2019) 114–123, https://doi.org/10.1016/j.surfcoat.2019.03.023.
[17] L. Pezzato, L. Lorenzetti, L. Tonelli, G. Bragaggia, M. Dabalà, C. Martini, K. Brunelli, Effect of SiC and borosilicate glass particles on the corrosion and tribological behavior of AZ91D magnesium alloy after PEO process, Surf. Coat. Technol. 428 (2021), 127901, https://doi.org/10.1016/j.surfcoat.2021.127901.
[18] Y. Gao, Y. Morisada, H. Fujii, J. Liao, Dissimilar friction stir lap welding of magnesium to aluminum using plasma electrolytic oxidation interlayer, Mater. Sci. Eng. A 711 (2018) 109–118, https://doi.org/10.1016/j.msea.2017.11.034.
[19] S. Aliasghari, A. Rogov, P. Skeldon, X. Zhou, A. Yerokhin, A. Aliabadi, M. Ghorbani, Plasma electrolytic oxidation and corrosion protection of friction stir welded AZ31B magnesium alloy-titanium joints, Surf. Coat. Technol. 393 (2020), 125838, https://doi.org/10.1016/j.surfcoat.2020.125838.
[20] S. Aliasghari, A. Němcová, P. Skeldon, G.E. Thompson, Influence of coating morphology on adhesive bonding of titanium pre-treated by plasma electrolytic oxidation, Surf. Coat. Technol. 289 (2016) 101–109, https://doi.org/10.1016/j.surfcoat.2016.01.042.
[21] A.G. Rakoch, A.A. Gladkova, Z. Linn, D.M. Strekalina, The evidence of cathodic micro-discharges during plasma electrolytic oxidation of light metallic alloys and micro-discharge intensity depending on pH of the electrolyte, Surf. Coat. Technol. 269 (2015) 138–144, https://doi.org/10.1016/j.surfcoat.2015.02.026.
[22] L. Pezzato, D. Vranescu, M. Sinico, C. Gennari, A.G. Settimi, P. Pranovi, K. Brunelli, M. Dabalà, Tribocorrosion properties of PEO coatings produced on AZ91 magnesium alloy with silicate- or phosphate-based electrolytes, Coatings 8 (2018) 202, https://doi.org/10.3390/coatings8060202.
[23] M. Ostapiuk, M.G. Taryba, L.M. Calado, J. Bieniaś, M.F. Montemor, A study on the galvanic corrosion of a sol-gel coated PEO mg-CFRP couple, Corros. Sci. 186 (2021), 109470, https://doi.org/10.1016/j.corsci.2021.109470.
[24] C. Ye, X. Chen, L. Wang, W. Peng, W. Zhu, W. Dong, B. Wang, SE, X. Li, Highly enhanced joint strength of direct-injection-moulded polyphenylene sulphide-magnesium composite by PEO coated interface, Surf. Coat. Technol. 404 (2020) 126565, https://doi.org/10.1016/j.surfcoat.2020.126565.
[25] N.K. Akafuah, S. Poozesh, A. Salaimeh, G. Patrick, K. Lawler, K. Saito, Evolution of the automotive body coating process-a review, Coatings 6 (2016) 24, https://doi.org/10.3390/coatings6020024.
[26] M. Reichinger, W. Bremser, M. Dornbusch, Interface and volume transport on technical cataphoretic painting: a comparison of steel, hot-dip galvanised steel and aluminium alloy, Electrochim. Acta 231 (2017) 135–152, https://doi.org/10.1016/j.electacta.2017.02.013.
[27] P. Cerchier, L. Pezzato, C. Gennari, E. Moschin, I. Moro, M. Dabalà, PEO coating containing copper: a promising anticorrosive and antifouling coating for seawater application of AA 7075, Surf. Coat. Technol. 393 (2020), 125774, https://doi.org/10.1016/j.surfcoat.2020.125774.
[28] C. Rossignol, N. Vialas, US 2021/0262107 A1, 2021.
[29] X. Ma, C. Blawert, D. Höche, K.U. Kainer, M.L. Zheludkevich, A model describing the growth of a PEO coating on AM50 mg alloy under constant voltage mode, Electrochim. Acta 251 (2017) 461–474, https://doi.org/10.1016/j.electacta.2017.08.147.
[30] Q. Li, J. Liang, B. Liu, Z. Peng, Q. Wang, Effects of cathodic voltages on structure and wear resistance of plasma electrolytic oxidation coatings formed on aluminium alloy, Appl. Surf. Sci. 297 (2014) 176–181, https://doi.org/10.1016/j.apsusc.2014.01.120.
[31] M. Mohedano, R. Arrabal, B. Mingo, A. Pardo, E. Matykina, Role of particle type and concentration on characteristics of PEO coatings on AM50 magnesium alloy, Surf. Coat. Technol. 334 (2018) 328–335, https://doi.org/10.1016/j.surfcoat.2017.11.058.
[32] G. Rapheal, S. Kumar, N. Scharnagl, C. Blawert, Effect of current density on the microstructure and corrosion properties of plasma electrolytic oxidation (PEO) coatings on AM50 mg alloy produced in an electrolyte containing clay additives, Surf. Coat. Technol. 289 (2016) 150–164, https://doi.org/10.1016/j.surfcoat.2016.01.033.
[33] J. Yang, C. Blawert, S.V. Lamaka, D. Snihirova, X. Lu, S. Di, M.L. Zheludkevich, Corrosion protection properties of inhibitor containing hybrid PEO-epoxy coating on magnesium, Corros Sci. 140 (2018) 99–110, https://doi.org/10.1016/j.corsci.2018.06.014.
[34] N. Godja, N. Kiss, C. Löcker, A. Schindel, A. Gavrilovic, J. Wosik, R. Mann, J. Wendrinsky, A. Merstallinger, G.E. Nauer, Preparation and characterization of spark-anodized Al-alloys: physical, chemical and tribological properties, Tribol. Int. 43 (2010) 1253–1261, https://doi.org/10.1016/j.triboint.2010.01.007.